ARTICLE

Ab initio Study of Complexation Process between Poly(amido-amine) and Nano-Silicon Dioxide

Tao Jin[a*], Hai-liang Lü[b]

a. College of Material Science and Engineering, Shandong University of Science and Technology, Qingdao 266590, China
b. College of Chemistry and Environmental Engeering, Shandong University of Science and Technology, Qingdao 266590, China

(Dated: Received on January 21, 2013; Accepted on April 15, 2013)

To understand better the molecular-level details of $\equiv Si^+$ (SC) or $\equiv SiO^-$ (SOA) ion group to -NH_2 teminated poly(amido-amine) dendrimers in the gas phase, density functional theory is used to optimize the minimum energy and transition state structures with UB3LYP/6-311G(d) and HF/6-31G levels. The tertiary amine nitrogen and the amide oxygen are found to be the most favorable binding sites. The activation energies of the different active sites and the reaction steps of SC and/or SOA ion group and the amide sites are also analyzed. The stable compounds are formed via the electrostatic interaction and the coordination effect. The orientation of the amide O and the rotation of the branches minimizes the energy of the whole system.

Key words: Polyamidoamine, Activation energy, Transition state, Density functional theory

I. INTRODUCTION

Polyamidoamine (PAMAM) dendrimers were synthesized for the first time by Tomalia *et al.* in 1985 [1]. These dendrimers have been successfully used as template agents for several ions, metal atoms and nanoparticle clusters, including Pt, Pd, Au, Ag, and Cu [2−6]. These dendrimers are tree-like, three-dimensional polymers, possessing three architectural components: a core, an interior, and a surface. The hydrophilicity or hydrophobicity of the terminal groups of the dendrimers can be modified based on different requirements. Therefore, dendrimers are suitable as medical materials [3], surfactants [5, 6], supports for organic synthesis [7], and chemical modifiers of silica surfaces [8−13]. Nano-silica is a useful filler in preparing water-based coatings, and pigments [14]. However, the modification dispersants are expected to bind to the surface possibly via hydrogen bonds, electrostatic interactions, and/or covalent bonds. Several microscopic adsorption mechanisms have been put forward in Refs.[15, 16], such as chemical bonding [17] and coordination theory [2]. But a definite mechanism has not yet emerged from the previous discussions [2, 15]. These theories cannot indicate a specific combination mode and a measurable energy value between modifier molecules and nanoparticles. Moreover, these qualitative theories cannot also faultlessly explain the Zeta potential (ξ) changes of the modified nanoparticles in slurry, compared with those of the unmodified nanoparticles. These changes reflect the dispersion stability of the modified nanoparticles in the dispersed medium. Therefore, the adsorption mechanism remains unresolved [2], and a quantitative study on the charge distribution and energy change is theoretically more important than a qualitative study [14]. Our previous study of the modification mechanism reveals that the binding of PAMAM and nano-silica is thermodynamically feasible, in close agreement with previous experiments [8−13]. We used the simple models [14, 18−22]: the cleavage of Si−O bonds in crystalline silica can produce four types of surface sites (*i.e.* $\equiv Si^{\cdot}$, $\equiv SiO^{\cdot}$, $\equiv Si^+$, and $\equiv SiO^-$, where $\equiv$ indicates the remaining three Si−O bonds attached onto the surface atom Si to the bulk solid. SC, SOA, SR, and SOR nomenclatures stand for $\equiv Si^+$, $\equiv SiO^-$, $\equiv Si^{\cdot}$, and $\equiv SiO^{\cdot}$, respectively). The different complexation configurations were obtained by optimizing the initial complexes of the heterolytic cleavage products and one branch of PAMAM-G0-NH_2 [23] in gas phase. The different chemical interaction modes were also analyzed, and the most stable configurations were due to the formation of Si−N^o and/or Si−O bond, respectively. However, our previous work only paid attention to the analysis on the complexation configurations, such as the change of the bond lengths and bond angles. The energy changes during the complexation process were not studied, moreover, the characteristics of these favorable binding sites of one branch of G0-NH_2 [5, 18, 27, 30] were not yet analyzed,

*Author to whom correspondence should be addressed. E-mail: jintaoqiao@163.com

including the amine nitrogen (N^o), the amide nitrogen and oxygen (N^a and O), as mentioned in our previous work [18]. The binding modes between one branch of G0-NH_2 and nano-silica were investigated on the basis of the symmetric structures and the similar properties of the active sites (N^o, N^a, and O).

However, the neighbouring branches of PAMAM dendrimers can affect the orientation of carbon-nitrogen chain each other. As mentioned before [5, 18], it is very possible to form the intrabranch N−H···N−H interactions or N−H···O=C interactions because of the shorter distance of two neighbouring branches. The hydrogen bond interaction makes the two -NH_2 terminated groups turn inward to keep stability and minimum energy. Thus, the calculated binding energy (ΔG) contains the rotation energy of the branches. To reduce the effect of the branches on the interaction of the active sites and nano-silica, only two branches (Fig.1 (1a) and (2a)) are used to study the interaction modes and the energy changes during the complexation process in this work.

In addition, composites of PAMAM and silica crystalline macromolecules need larger computer memory and longer calculation time, and a simplified silica surface model [5, 18, 30] is necessary. The lowest-generation dendrimers may provide valuable details about the mechanisms of nanoparticles attachment to the dendrimer sites. Molecular structural models including classical molecular dynamics (MD), quantum density functional theory (DFT), Hartree-Fock (HF), as well as coarse-grained methods, have been used to determine the structural and dynamical characteristics of the low-order generation dendrimers. Therefore, the present study focuses on the interaction between the lowest-generation G0-NH_2 and nano-silica in the gas phase. The effect of the solvent on the interaction energy had been discussed in another work [27] (CPCM model was used to analyze the interaction effect). To achieve a thorough understanding of the geometrical structures and electronic properties of $\equiv Si^+$ (SC) or $\equiv SiO^-$ (SOA) ion complexation to the most favorable dendrimer sites, and better to understand the results obtained from the experiments, therefore, in this work, we investigate the interaction details and energy changes during the complexation process, such as the reaction modes, the activation energy, and reaction steps.

II. METHODOLOGY

A simplified model of silica surfaces was created by considering a limited number of atoms around the active surface sites. This type of model has been successfully used before [5, 18, 24−30]. Figure 1 illustrates the fragments of G0-NH_2 and the modeled surface sites in this work. Models (1a) and (2a) of Fig.1 are two branches of G0-NH_2. Model (1a) of Fig.1 contains one core nitrogen atom (N^c, nomenclature in Table I), and model

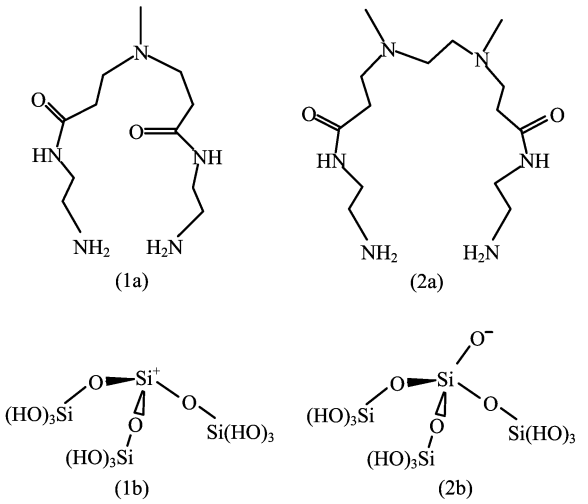

FIG. 1 Model fragments of PAMAM dendrimer and heterolytic cleavage fragments of nano-SiO_2 used in this work [5, 18]. (1a) One amine nitrogen (N^c) in core region, one oxygen (O) orients outwardly, while the other orients inwardly, ((1a) fragment is termed PF43, PF stands for PAMAM fragment and the two-digit number indicates the number of atoms that composes the fragment). (2a) Two N^c in the ethylenediamine (EDA) core region, two amide O all orients outwardly in both branches ((2a) fragment is termed PF54, the meaning of PF54 is the same as that of PF43). (1b) The heterolytic cleavage: $\equiv Si^+$ termed as SC ion. (2b) The heterolytic cleavage: $\equiv SiO^-$ termed as SOA ion.

(2a) of Fig.1 has the ethylenediamine (EDA) core group (=N−CH_2CH_2−N=). Models (1b) and (2b) of Fig.1 [18, 24, 27] are heterolytic cleavage fragments of nano-SiO_2 due to the mechanical clash interaction, friction force, and shear force. Models (1b) and (2b) of Fig.1 consist of a central Si ion or Si−O ion groups designating the surface sites and three $(OH)_3SiO$ groups mimicking the subsurface bonding. Although the above-mentioned model is not a perfect representation of the silica surface, these molecules are reasonable representations of silica-surface functional groups.

Initial optimizations were performed at the Hartree-Fock (HF) level and the basic 3-21G basis set for PAMAM molecule. Then, to fully optimize these fragments without symmetry incorporating electron correlation, the larger basis sets (HF/6-31G(d) and HF/6-311G(d)) were performed to improve the calculated results. To gain insights into the effect of silica surface active sites on the mechanism between PAMAM and silica powder, three $(OH)_3SiO$ groups were assumed to be frozen to prevent the effect of the hydroxyl groups on the configuration. Of course, the effect of the steric hindrance was inevitable and significant and was thus taken into account.

The relevant binding energies and charge states were calculated using DFT approach based on the Becke's three-parameter exchange functional with the Lee-Yang-Parr correlation functional (B3LYP) [28, 30, 31].

DOI:10.1063/1674-0068/26/03/277-286

TABLE I Gibbs free energy (ΔG)[a] of the complexation process of SC and the dendrimer fragment [18] according to Eq.(1) with B3LYP/6-311G(d)//HF/6-31G(d) theory level.

Species	Various binding sites	ΔG/(kJ/mol)	$\Delta\Delta G_{(\mathrm{rel})}$/(kJ/mol)
PF43-SC	Amine N^c (in core)	−289.04	113.78
	Amine N^o (in teminated group)	−391.73	11.09
	Amide N^a (in amide group)	−283.35	119.47
	Amide O (in amide group)	−402.82	0.00
PF54-SC	Amine N^c (in core)	−273.35	123.02
	Amine N^o (in teminated group)	−388.54	7.83
	Amide N^a (in amide group)	−279.54	116.83
	Amide O (in amide group)	−396.37	0.00

[a] $\Delta G = G_{\text{SC-X-fragment}} - G_{\text{SC}} - G_{\text{X-fragment}}$; $\Delta\Delta G_{(\mathrm{rel})}$ is the relative ΔG, and the minimum ΔG is assumed to be zero-point energy as the reference value in order to compare the differences easily.

The energies of reactants and products were minimized without any constraints. Stationary points on the potential energy surface were verified by full frequency analysis. Single-point potential energy calculations were also performed with the UB3LYP/6-311G(d). The minmum energies and transition state (TS) structures of the relevant systems used in the present work were also optimized at the UB3LYP/6-311G(d) level of theory, and the existence of true local minimum was tested in all cases. The binding energies (ΔE) were determined through hybrid DFT single point calculations on the HF fully optimized geometries. The geometrical structures were well represented through optimization, as indicated by our analysis of bond lengths, bond angles, and dihedrals [5, 18, 27]. The enthalpy (ΔH) and Gibbs free energy (ΔG) of the complexation process were also calculated. TS structures were located by running either a Berny optimization to a saddle point, traditional TS search, or using the synchronous transit-guided quasi Newton (STQN) method or both [28]. In this work, the traditional TS search method was used at the 6-31G(d) basis set level. The transition states of various possible reaction pathways were obtained and verified by internal reaction coordinate (IRC) analysis. The activation energy (E_a) was defined as the difference in enthalpy (H) of the relevant states. None of the calculated structures for SC-G0-NH_2 had stable states with spin multiplicities higher than 1, and the same method and basis sets (UB3LYP/6-311G(d)//HF/6-31G(d)) were used to calculate these species, as mentioned previously [5, 18, 27, 30].

Finally, to determine the role of tertiary amine and amide sites in one branch of dendrimers, DFT optimization was performed by placing an SC ion near one active site atom (N or O) from above or below the plane, which was composed of carbon-nitrogen chains, approximately coplanar. Nano-SiO_2 prefers the combination of the amide site. Therefore, we investigate the chemical details of the amide site based on the G0-NH_2 *trans* configuration. The SC cation group is gradually placed near the amide O active site from around the oxygen (from below the carbon-nitrogen chain or from the side of the carbon-nitrogen chain), SOA ion group is placed next to one carbon-nitrogen chain. The final configurations are optimized by UB3LYP/6-311G(d)//HF/6-31G(d)) basis sets. Figure 2 is presented here to illustrate the general procedure followed in other sections.

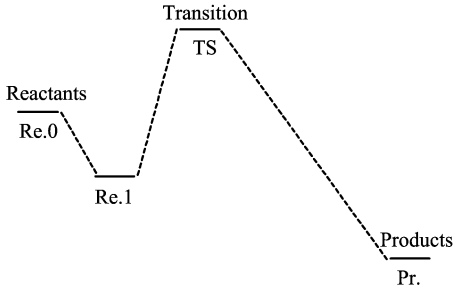

FIG. 2 Diagram of the reaction process of PAMAM fragment (PF43 and/or PF54, SC and/or SOA) guest [28].

III. RESULTS AND DISCUSSION

A. Determination of the most favorable binding sites for complexation of SC ion group

Binding of SC ion to the tertiary amine nitrogen (N^o), the secondary amide nitrogen (N^a), and the amide oxygen (O) of PAMAM dendrimers had been investigated [18, 27, 30]. Therefore, several structures are calculated in this work, and solventless complexation of SC ion to the active sites of the dendrimers follows three steps. First step is a free energy-reducing process (state Re.0→state Re.1) (see Fig.2), where the electrostatic induction force (or attractive force) and/or van del Waals force influence the energy changes, and the second step corresponds to a thermally activated process with the activation energy increasing (state Re.1→ state TS), where the electrostatic repulsion force influ-

DOI:10.1063/1674-0068/26/03/277-286

TABLE II Activation energies (E_a) of reaction process for SC and the active oxygen sites according to Eq.(2) with B3LYP/6-311G(d)//HF/6-31G(d).

Species	E_a/(kJ/mol)	$\Delta E_{a(rel)}$/(kJ/mol)	ΔG/(kJ/mol)
CH_3CH_2OH	46.88	5.86	−430.74
$CH_3CH_2CONH_2$	41.02	0.00	−406.46
$CH_3CH_2CONH_2CH_2CH_3$	55.67	14.65	−403.95
$NH_2(CH_2)_2CONH(CH_2)_2NCH_3$	86.65	45.63	−401.02
$(NH_2(CH_2)_2CONH(CH_2)_2)_2NCH_3$ (*i.e.* PF43)	99.63	58.60	−402.69
$(NH_2(CH_2)_2CONH(CH_2)_2)_2(NCH_3CH_2)_2$ (*i.e.* PF54)	101.30	60.28	−396.41

E_a=$\Delta H_{TS.\text{-}Re.1}$ (see Fig.2), $\Delta E_{a(rel)}$ is also the relative E_a.

ences the energy changes, accompanied by the configuration changes of the complexes. The third step is the energy-releasing process (state TS→state Pr) to obtain the stable states, which can be either endo- or exothermic process. The overall complexation process can be represented by Eq.(1):

$$\text{Fragment-X} + \text{SC} \rightarrow (\text{Fragment-X-SC})^{\neq} \rightarrow \text{Fragment-X-SC} \qquad (1)$$

where X stands for the active sites of PAMAM dendrimers: the amine sites, nitrogen (N^c or N^o), the amide sites, nitrogen (N^a), and oxygen (O). Thus, the equation is a general formula to show the reaction process. The Gibbs free energy (ΔG) of the different active sites and nano-silica during the complexation process are showed in Table I.

To understand how the different branches affect the complexation process of SC ion group (guest) bound to the active sites of PAMAM fragments (host), we also modeled a dendrimer branch with a 43-atom fragment (PF43) and an outer pocket with a 54-atom PAMAM fragment (PF54), such as $(NH_2(CH_2)_2NHCO(CH_2)_2)_2NCH_3$ (*i.e.* Fig.1(1a)) and $(NH_2(CH_2)_2NHCO(CH_2)_2(NCH_3)_2)_2(CH_2)_2$ (*i.e.* Fig.1(2a)), respectively. The outer pocket fragment (PF54) consists of two dendrimer branches stemming from a tertiary amine nitrogen (N^c) and terminated in -NH_2 group. One of those branches including the tertiary amine nitrogen site makes up the single branch model (PF24, see Table II). Although Fig.2 depicts a TS structure between Re.1 and Pr., no TS search is performed in this section because we only study the characteristics of the active sites in the different branches. Moreover, the effect of the solvent on TS structure is not considered due to the paper length limitations, and this work will be accomplished in another work.

The results indicate that the amide O and the amine nitrogen (N^o) are the most favorable sites bound to SC ion group, and the ΔG values for PF43-SC complex are −402.82 and −391.73 kJ/mol, respectively. The secondary combining sites are the amide nitrogen (N^a) and the amine nitrogen (N^c). But the order of binding is not consistent with a variety of dendrimer fragments. From Table I it can be seen that $O>N^o>N^c>N^a$ for PF43 fragment, however, the order changes to $O>N^o>N^a>N^c$ for PF54 fragment. Nonetheless, the difference between the ΔG for the binding to the amide N^a and binding to the amine N^c is not significant. The difference is 5.69 kJ/mol for PF43-SC complex and 6.19 kJ/mol for PF54-SC complex, respectively. Thus, it can be affirmed that binding to the amide N^a is as basically feasible as binding to the amine N^c. The rule is also applicable to the amide O and the terminal N^o groups, and the relative ΔG ($\Delta\Delta G$) is not also significant, such as 11.09 kJ/mol for PF43-SC complex, and 7.83 kJ/mol for PF54-SC complex. From all the sites tested, it is obvious that complexation of SC to the amide O and the terminated N^o group is the most likely type of binding (see Fig.3). These calculations show that the chemical binding of SC group to the active sites is feasible, in accordance with our previous works [27]. The stronger electronegativity of O atom (3.5) and N atom (3.07) contributes to the formation of the stronger chemical binding, compared to the electronegativity of carbon atom (2.5) [18, 24].

Our results also indicate that the effect of the different branches to ΔG is obviously different, for instance, the difference of ΔG for the binding to the core N^c in particular. The ΔG value for PF43-SC complex is −289.04 kJ/mol, compared with −273.35 kJ/mol for PF54-SC complex. Thus, the binding to the single core N^o atom of PF43 fragments is more feasible than that to the two core N^o atoms of PF54 fragments. For PF43-SC complex, the most binding mode is from below the planar composing of the two branches, as shown in Fig.3, because the steric hindrance of this combination mode is very weak. However, for PF54-SC complex, the binding to the core nitrogen atoms should be the most stable binding mode due to two core N^o atoms. In fact, the two neighboring carbon-nitrogen chains are non-planar when SC is bound to the core region, because the carbon-nitrogen chains can be distorted or transformed by SC guest. As mentioned in Refs.[27, 28], the N−C−C−N core dihedral angle up to 180° may allow larger guest to be hosted, moreover, the two core nitrogen atoms show higher electronega-

DOI:10.1063/1674-0068/26/03/277-286

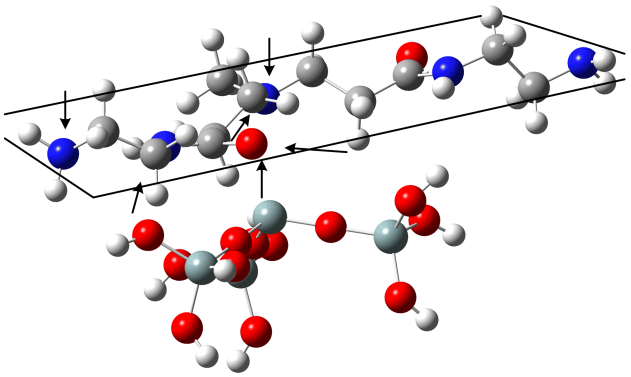

FIG. 3 The different binding mode between PF43 fragment and SC group, the arrows indicate the binding direction.

tivity and stronger coordination to SC ion group [18]. Therefore, the competitive adsorption of the two nitrogen atoms to SC ion group can make the average N^c-C (in core region) bond length change to 1.459 Å (The value of N−C bond length is 1.462 Å [30]) due to the higher electron cloud density. Thus, when SC ion group is bound to the core active site, the steric hindrance is nonnegligible due to the carbon-nitrogen chain distortion. Moreover, the change of the bond length and bond angle also produces the energy consumption.

B. Analysis of E_a and the reaction steps for complexation of SC ion group with the most likely binding site

In the following section, the complexation process of SC and the amide oxygen site (O) is discussed using the same method and basis sets, as mentioned above. TS structures and E_a are calculated to analyze the kinetic effect. The thermodynamic analysis approach ought to be used to understand the characteristic of the most favorable binding sites. As analyzed before, the dendrimer fragment can affect the binding characters of SC and the active sites. As it is important to understand how the complexation of SC ion group takes place, we focus our attention on studying the thermodynamic aspects of the binding process. To understand the characters of the most favorable site (O) in detail, the different dendrimer fragments are used to search for TS precursors and to calculate E_a. This molecular fragments all contain the oxygen atom (O), such as CH_3CH_2OH, $CH_3CH_2CONH_2$, $CH_2CH_2CONH_2CH_2CH_3$, PF43, $NH_2(CH_2)_2NHCO(CH_2)_2NCH_3$, and PF54 (*i.e.* Fig.1 (1a) and (2a)). Therefore, the effect of the different fragments on E_a is emphasized. The calculated values for E_a are shown in Table II.

Having observed that the amide O is the most favorable site for binding, we extend the thermodynamic analysis of G0-NH_2-SC complexes to the hydroxyl (-OH) and/or the amide (-$CONH_2$) complexes. The calculated results indicate that the amide oxygen has the stronger binding ability (see Table II), but the characteristics of the oxygen (O) bound to SC ion group are affected by the different molecular fragments. The calculated TS structures and activation energies are analyzed to assess the kinetic effect. The oxygen (O) site is modeled with the different branches (see Table II), making us to evaluate the effect of the branch on E_a.

The reaction process is given by Eq.(2):

$$\begin{aligned} F-O+{}^{+}Si\equiv &\rightarrow (F\cdots O\cdots Si\equiv)^{+} \\ &\rightarrow (F\cdots O-Si\equiv)^{+} \end{aligned} \qquad (2)$$

where F is delegated to stand for the atoms (or groups) bound to O. This Eq.(2) obviously indicates that the amide oxygen active site (O) is different from Eq.(1). Although numerous reaction profiles could be traced, we attempted to describe at least one starting from the lowest energy configuration of Re.1 all the way down to the lowest energy configuration of the final products (Pr.) [28]. However, the calculation of the full reaction profile of all the intermediates and TS structures has not been possible for all SC-O-F complexes due to the structural complexity and diversity [28], and the TS structure was calculated for the selected configurations using the known geometric parameters.

1. Analysis of E_a in complexation process

TS structure was calculated with Berny optimization of a trigonal-bipyramidal-like TS structure [28, 30]. Re.1 and Pr. Structures were obtained by optimization of initial configuration set up by subtracting or adding a fraction of the imaginary frequency displacement vector from the TS atomic coordinates, respectively. Firstly, Re.1 structure could be derived directly from TS structure optimization, because no displacement leading to a branch rotation is found in the TS displacement vector in the forward direction. Secondly, no stable intermediates could be found either between Re.1 and TS or between TS and Pr.. Thus, the results show that the lowest E_a is 41.02 kJ/mol for a single molecular $CH_3CH_2CONH_2$. The secondary activation energy is 46.88 kJ/mol for the ethanol molecular CH_3CH_2OH. However, the ΔG for SC ion bound to hydroxyl group (-OH) is the lowest. The ΔG value is −430.74 kJ/mol indicating the better stability. Therefore, this suggests that the reaction will be easier to perform with the hydroxyl group or the amide group, according to Eq.(2). However, when the alkyl group (-CH_2CH_3) is bound to the amide site, E_a increases 14.65 kJ/mol, compared to that for $CH_3CH_2CONH_2$. As shown in Table II, the reaction for SC bound to $NH_2(CH_2)_2CONH(CH_2)_2NCH_3$ is more difficult due to the higher E_a (86.65 kJ/mol). The change of E_a is smaller for PAMAM fragments. The relative activation energies (ΔE_a) is 58.6 and 60.28 kJ/mol for PF43 and PF54, respectively.

DOI:10.1063/1674-0068/26/03/277-286

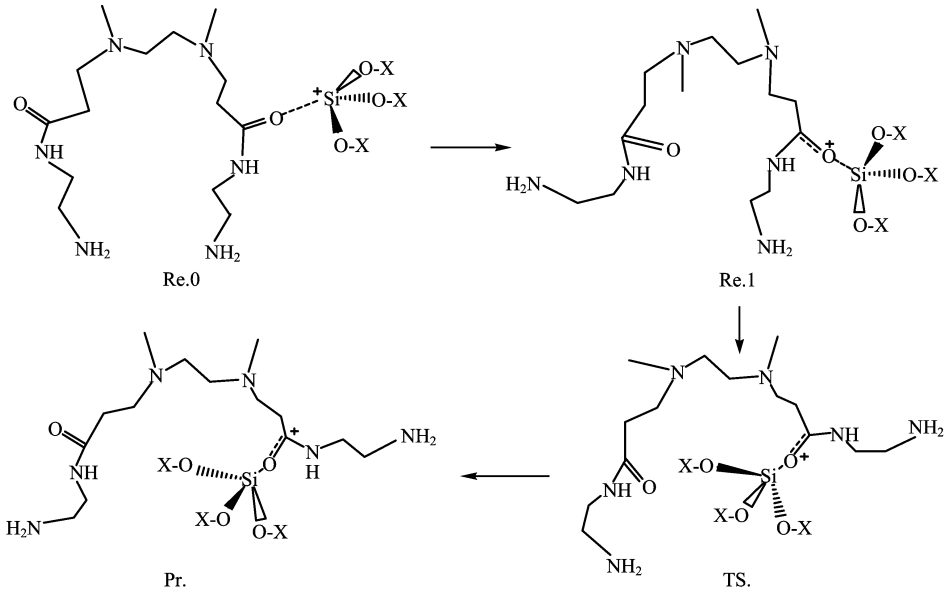

FIG. 4 Stable points along the solventless reaction path of SC and the amide O, X stands for the -Si(OH)$_3$ group.

Thus, a few sights are gained. Firstly, the molecular weight of the reactant systems and the characteristics of these groups markedly affect the reaction process and E_a such as -NH_2, -NCH_3, and -$NH(CH_2)_2NCH_3$. Secondly, the reaction activities of between hydroxyl oxygen (O) and SC ion group and between carbonyl oxygen (O) and SC ion group are obviously different. The E_a of SC bound to $OHCH_2CH_3$ is 5.86 kJ/mol which is more difficult compared with that of SC bound to $OCNH_2CH_2CH_3$. For hydroxyl O, there are a lone pair of electrons among extra-nuclear electrons, suggesting the high nucleophilicity. And for carbonyl O, there are a carbon-oxygen double bond and an amino group bound to carbonyl carbon (O=C(R)−NH_2, R stands for the other alkyl group bound to carbonyl carbon), moreover, the p-π conjugation effect makes the electron delocalization in the amine sites, that is to say, the electrons in 2p orbital of nitrogen atom also contribute to this electron effect. Therefore, the whole molecular becomes more stable and this binding between the carbonyl oxygen (O) and SC ion group is also easier due to the higher electron cloud density in the amide active site (O=C(R)−N−). Thus, the E_a of SC bound to $OCNH_2CH_2CH_3$ is the lowest, as analyzed above. However, the reaction becomes more and more difficult with the increase of molecular weight of carbon-nitrogen chains. The energy consumption is also evidently attributed to the steric hindrance effect. ΔE_a is more than 45.63 kJ/mol when one carbon-nitrogen chain is at least introduced, then, ΔE_a value increases more than 58.6 kJ/mol when two carbon-nitrogen chains are introduced (for example, PF43 and PF54 dendrimer fragments). Of course, the rotation of the carbon-nitrogen branch is necessary to minimize the repulsion between the molecular host and SC guest group in the final product structures, and elsewhere we show that such repulsion could require the presence of explicit solvent in order to minimize the energy of the SC-fragment complexes [27].

2. Complexation process of SC ion group and the amide sites of PF54 dendrimers

The larger number of atoms results in the difficulty of a snapshots of collection of both the reactants and the products due to a number of isomeric configurations, also making difficult the tracing of the reaction profile. Modeling the complicated branches with the amide sites is more challenging than modeling a single site molecule like $OHCH_2CH_3$. To obtain the reaction details of SC ion group and the amide sites, we modeled two dendrimer branches with a 54-atom fragment (PF54), which stemmed out from a tertiary amine nitrogen (N^c) just like an outer pocket. The carbon-nitrogen chains can not only provide the interaction details of the amide sites, but also show the effect of branches on the stability of the products based on the previous analysis [5, 18, 27, 30]. In this section, the reaction profile is described by the following equations, starting with the product PF54-SC obtained according to Eq.(1) with the ΔG=279.54, 396.37 kJ/mol. The reactants and products are represented in Fig.4. The changes of energies (including zero-point energy correction (ΔE), ΔH, and ΔG), Si−O distances, and C=O bond lengths in complexation process are shown in Table III and Fig.5.

The step 1 for reaction process is given by Eq.(3), accommodation of SC beside the branch.

$$\mathrm{PF53-O} + {}^{+}\mathrm{Si} \equiv \rightarrow (\mathrm{PF53}\cdots\mathrm{O}\cdots{}^{+}\mathrm{Si}\equiv) \qquad (3)$$

PF54 is changed into PF53−O for highlighting the ac-

DOI:10.1063/1674-0068/26/03/277-286

TABLE III Difference in electronic energy with zero-point energy correction (ΔE), enthalpy (ΔH), and Gibbs free energy (ΔG) of complex reaction optimized at B3LYP/6-311G(d)//HF/6-31G(d), and the change of Si$\cdots$O distances and C=O bond lengths during the complexation process of SC and PF54 fragments.

Stationary point	ΔE/(kJ/mol)	ΔH/(kJ/mol)	ΔG/(kJ/mol)	Si$\cdots$O distance/Å	C=O bond length/Å
Re.0	−24.7	−28.05	−26.37	2.258	1.230 [30, 31]
Re.01	−105.07	−113.02	−108.0	1.945	1.245
Re.1	−31.81	−34.33	−32.65	1.789	1.261
TS.	73.67	87.07	97.95	1.768	1.278
Pr.1	−59.86	−61.12	−59.44	1.744	1.299
Pr.	−174.56	−175.39	−169.95	1.732	1.282

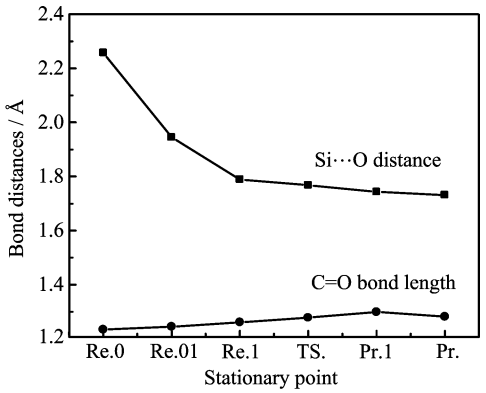

FIG. 5 Evolution of Si$\cdots$O distances and C=O bond length along the reaction course.

tive oxygen (O), the other nomenclatures are termed in Fig.1. To show clearly the formation course of new bond (Si−O) and describe better the different stationary points along the reaction profile, the distance of Si and O atom was about 2.26 Å in the initial configurations of SC and PF54 dendrimer. If the initial configuration was unreasonable, we could not gain the better results. This step (Re.0→Re.01→Re.1) is shown in Fig.2 and Fig.4. During this step, the electrostatic attraction will play a major role in the absorption of SC ion to the host molecular. Of course, no TS structure was again calculated between stationary points, and the first step above (see Fig.4 and Table III) is taken into about, thus, ΔH (the sum of ΔH in this step (*i.e.* Re.0→Re.01→Re.1, see Table III)) and ΔG (the sum of ΔG in this step (*i.e.* Re.0→Re.01→Re.1, see Table III)) are −175.4 and −167.02 kJ/mol, respectively. Obviously, this step is thermodynamically favorable due to the exothermic process. The orientation of the amide O atom in the neighboring carbon-nitrogen branch changes from outward (see Re.0 state in Fig.4) to inward (see Re.1 state in Fig.4), and the terminated NH_2 group orients outward keeping the *trans* configuration. During the complexation process, the rotation of carbon-nitrogen chain reduces the repulsion and increases the interior space to accommodate SC guest group. The ΔG of −108.0 kJ/mol (it corresponds to Re.01 stationary point) shows that this step makes the energy of the whole system reduce markedly.

The step 2 for reaction process is given by Eq.(4), weak binding of SC and the amide O

$$(\mathrm{PF53}\cdots\mathrm{O}\cdots{}^{+}\mathrm{Si}\equiv) \rightarrow (\mathrm{PF53}\cdots\overbrace{\mathrm{O}\cdots\mathrm{Si}}^{+}\equiv) \quad (4)$$

As shown in Fig.4, the orientation of the terminated -NH_2 group in the neighboring chain changes back to inward (TS.), indicating the *cis* configuration. The carbonyl group bound to SC ion group orients downward due to the strong electrostatic interaction and the rotation effect of carbon-nitrogen branch, and the terminated -NH_2 group bound to SC ion group orients outward, keeping the *trans* configuration. The guest SC ion group is accommodated into the "pocket" of the host molecular. For this step, the changes of the distance between Si and O and the carbonyl bond length are evident. The distance of Si and O changes from 2.26 Å to 1.768 Å, and the weak binding (the value of 1.768 Å [18] for the bond length of Si and O is the receivable) indicates that the new bond is to be formed. The C=O bond length changes also from 1.23 Å [27, 28] to 1.278 Å. The charge distribution of TS product is different from that of the initial reactants due to the charge transfer, as shown in Fig.4. The Mulliken atomic charge distribution is obtained using the same method (B3LYP/6-311G(d)//HF/6-31G). Once this step is complete, the complex compound is formed based on the positive charge transfer between SC group as donor and PF53-O molecular as acceptor. Upon the reaction, ΔH and ΔG are 87.07 and 97.95 kJ/mol, respectively. Therefore, this step is not thermodynamically favorable, and the increase of carbonyl bond length and the orientation of the terminated -NH_2 group mean the energy requirement. During this step, the binding process is endothermic to overcome the repulsion interaction among extranuclear electrons and the steric hindrance effect. In a word, the integrated electronic effect plays an important role in this step. Figure 5 illustrates the reaction profile and the evolution of the main distances in this process.

The step 3 for reaction process is given by Eq.(5), re-accommodation of SC ion group inside pocket and

DOI:10.1063/1674-0068/26/03/277-286

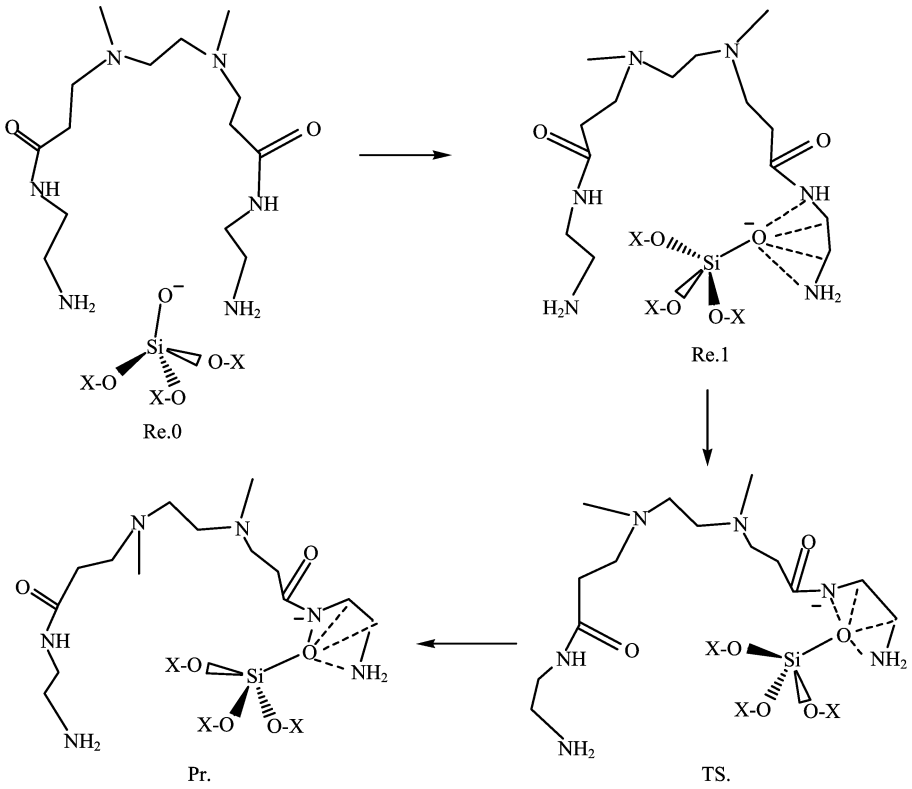

FIG. 6 Stable points along the solventless reaction path of SOA and the amide sites. X stands for the -Si(OH)$_3$ group.

rotation of branches

$$(\mathrm{PF53}\cdots\overbrace{\mathrm{O}\cdots\mathrm{Si}}^{+}\equiv)\xrightarrow{\text{Rotation of branches}}(\overbrace{\mathrm{PF53}\cdots\mathrm{O}-\mathrm{Si}\equiv}^{+}) \quad (5)$$

This step mainly involves the accommodation of SC ion group inside the pocket. The orientation of the terminated NH_2 group in the neighboring chain again changes back to outward (Pr.), indicating the *trans* configuration. Once the step is complete, the new Si−O bond of length 1.732 Å is finally formed, and the energy of the final product also reduces evidently. The energy release of ΔG (the sum of $\Delta G_{\mathrm{Pr.1\text{-}TS.}}$ and $\Delta G_{\mathrm{Pr.\text{-}Pr.1}}$) are −229.39 kJ/mol, therefore, this step is also thermodynamically favorable. However, it is noticeable that C=O bond length changes from 1.299 Å (stationary point: Pr.1) to 1.282 Å (the stable product: Pr.). One reason may be that the positive charge distributes more equably in the amide region, and the other reason may be that the neighboring group (-NHCH$_2$-) attracts the electrons of the carbonyl group due to the larger electronegativity of N atom. In sum, this change is attributed to the energy relaxation. The orientation of the amide O leads to the distortion and rotation of the chemical bonds, and the change also minimizes the energy of the final product. Thus, we speculate that the partial electron would delocalize around carbonyl O and amide N via induction effect of SC group, forming SC coordination to amide O and N. The analysis results indicate that the steric hindrance effect of SC groups and electrostatic repulsion is more prominent than the induction effect and the relative hydrogen bond interaction [18]. Therefore, the complex configurations are to be determined on the basis of the orientation of the amide O atom and the whole electron effect, which are caused by SC guest.

C. Complexation process of SOA ion group and the amide sites of PF54 dendrimers

In the following section, the complexation process of SOA and PF54 fragment of G0-NH$_2$ is focused on using the same method and basis sets as those in the preceding section. The polarizing power of SOA is weaker due to its larger size and full extranuclear electronic shell structure than SC [18]. Only carbonyl C and H atoms bound to carbon or nitrogen show electropositivity. Table IV shows the energy change during the complexation process of SOA and PF54 fragments. Thus, when the guest becomes close to the inner carbonyl C, the interactions between SOA and the dendrimers are investigated. SOA needs to overcome repulsion interactions from the negative charges of carbonyl O and amide N. To determine how SOA and hydrogen in the dendrimer terminal amine sites influence their complex configu-

DOI:10.1063/1674-0068/26/03/277-286

rations, DFT optimization is performed by placing an SOA anion near one amine H atom or in the middle of two amine nitrogens. The optimized configurations are shown in Fig.6. The optimized results indicate difficulty in obtaining the stable configuration for SOA-carbonyl C complexation, and SOA particularly preferred to the combination with H in the periphery. To determine the parameters affecting SOA and H interaction, the non-bonded distance and energy parameters are considered as initial values for the bond length and energy parameters. The optimized results show that a chemical coordination structure is easily formed between the PF54 fragment of G0-NH_2 dendrimer and SOA.

The reaction profile is described, starting with the product PF54-SOA obtained according to Eq.(6). The reactants and products are represented in Fig.6. The changes of energies (including ΔE, ΔH, ΔG, and $O\cdots N^a$ distances in complexation process are shown in Table IV and Fig.6).

The step 1 for reaction process is given by Eq.(6), accommodation of SOA beside the branch.

$$\mathrm{PF33-N^aH-CH_2-CH_2-N^oH_2+{}^-OSi} \equiv\rightarrow$$
$$\mathrm{PF33-\overbrace{N^aH-CH_2-CH_2-N^oH_2}^{-}\cdots OSi} \equiv \quad (6)$$

PF54 is changed into PF33−$N^aH_2CH_2CH_2N^oH_2$ for highlighting the active carbon-nitrogen branches, the other nomenclatures are termed in Fig.1.

To describe clearly the different stationary points along the reaction profile, the distance of O and N^a atom was about 3.258 Å in the initial configurations of SC and PF54 dendrimer. If this initial distance was unreasonable, and the stationary point energy could not be obtained. This step (Re.0→Re.01→Re.1) is shown in Fig.2 and Fig.6. During this step, the electrostatic attraction will play a major role in the absorption of SOA ion to the host molecular. Of course, no TS structure was again calculated between stationary points, and the first step above (see Fig.6 and Table IV) is taken into about, thus, ΔH (the sum of ΔH in this step (*i.e.* Re.0→Re.01→Re.1, see Table IV)) and ΔG (the sum of ΔG in this step (*i.e.* Re.0→Re.01→Re.1, see Table IV)) are −80.79 and −79.54 kJ/mol, respectively. Obviously, this step is also thermodynamically favorable due to the exothermic process. The orientation of the amide O atom in the neighboring carbon-nitrogen branch changes from outward (see Re.1 state in Fig.6) to inward (see TS. state in Fig.6), and the terminated -NH_2 group orients inward keeping the *cis* configuration. During the complexation process, the rotation of carbon-nitrogen chain reduces the repulsion and increases the interior space to accommodate SOA guest group. The ΔG of −24.7 kJ/mol (it corresponds to Re.01 stationary point) shows that this step makes the energy of the whole system reduce markedly.

The step 2 is weak coordination of SOA to H atoms of the carbon-nitrogen chain. As shown in Fig.6, the terminated -NH_2 group bound to SOA ion group also orients inward due to the coordination effect, keeping the *trans* configuration. However, the orientation of the terminated -NH_2 group in the neighboring chain indicates the *cis* configuration, and the carbonyl group orients downward due to the rotation effect of carbon-nitrogen branch. The guest SOA ion group is surrounded by the -$N^aH_2CH_2CH_2N^oH_2$ fragment of the G0-NH_2 dendrimer. For this step, the change of the distance between SOA ion group and the amide nitrogen (N^a) is evident. The distance of SiO and N^a changes from 3.258 Å to 2.189 Å, and the charge distribution of TS product is different from that of the initial reactants due to the charge transfer [18, 27], as shown in Fig.6. Once this step is complete, the complex compound is formed based on the negative charge transfer between SOA group as donor and PF54 molecular as acceptor. The coordination effect is also formed between SOA ion group and hydrogen (H) atoms in carbon-nitrogen chain, such as the amide hydrogen -N^aH-, the methylene hydrogen -CH_2-, and the amine hydrogen -N^oH_2-. Upon the reaction, ΔH and ΔG are 40.6 and 39.35 kJ/mol, respectively. Therefore, this step is not thermodynamically favorable too, and the orientation of the terminated -NH_2 group means the energy requirement. During this step, the binding process is also endothermic to overcome the repulsion interaction among extranuclear electrons and the steric hindrance effect. In a word, the integrated electronic effect plays an important role in this step. Figure 6 illustrates the reaction profile and the evolution of the main distances in this process.

The step 3 is re-accommodation of SOA ion group inside pocket and rotation of branches. This step mainly involves the accommodation of SOA ion group inside the pocket. Once the step is complete, the energy release of ΔG (the sum of $\Delta G_{\mathrm{Pr.1\text{-}TS}}$. and $\Delta G_{\mathrm{Pr.\text{-}Pr.1}}$) are −106.74 kJ/mol, therefore, this step is also thermodynamically favorable. However, it is noticeable that the distance of $O\cdots N^a$ changes from 2.195 Å (stationary point: Pr.1) to 2.189 Å (the stable product: Pr.), in better agreement with the expected value [18]. One reason may be that the negative charge distributes more equably in the amide region, and the other reason may

TABLE IV Difference in electronic energy with ΔE, ΔH, and ΔG of complex reaction optimized at B3LYP/6-311G(d)//HF/6-31G(d), and the change of $O\cdots N^a$ distances (in Å) during the complexation process of SOA and PF54 fragments. Energy values are given in kJ/mol.

	ΔE	ΔH	ΔG	$O\cdots N^a$ distance
Re.0	−26.37	−28.46	−27.63	3.258
Re.01	−23.02	−24.28	−24.70	2.745
Re.1	−26.79	−28.05	−27.21	2.348
TS.	38.51	40.60	39.35	2.207
Pr.1	−30.56	−30.98	−30.14	2.195
Pr.	−74.09	−79.12	−76.60	2.189

DOI:10.1063/1674-0068/26/03/277-286

be that the neighboring group (-$NHCH_2$-) attracts the electrons of the carbonyl group due to the larger electronegativity of N atom. In sum, this change is attributed to the energy relaxation. The orientation of the amide O leads to the distortion and rotation of the chemical bond, and the change also minimizes the energy of the final product. Thus, we speculate that the partial electron would delocalize around carbonyl O and amide N via induction effect of SOA group, forming SOA coordination to the H atoms in the amide sites. The analysis results indicate that the steric hindrance effect of SOA groups and electrostatic repulsion is more prominent than the induction effect and the relative hydrogen bond interaction [27]. Therefore, the complex configurations are to be determined on the basis of the orientation of the amide O atom and the whole electron effect, which are caused by SOA guest.

IV. CONCLUSION

The analysis of the interaction mechanism between PAMAM and nano-SiO_2 indicates the formation process of the chemical bond and the evolution profile of the complex configurations. The calculated results show that the amide O and the amine nitrogen (N^o) are the most favorable sites for the complexation of SC ion group. The activity of binding sites is affected by the dendrimer branches. The groups (such as -NH_2, -NCH_3, and -$NH(CH_2)_2NCH_3$) of the molecular fragments markedly affect the reaction process and the activation energies (E_a). The effect of the different branches on ΔG is also obviously different. SC binding to the single core N^o atom in PF43 is more feasible than that to the two core N^o atoms in PF54, and SC binding to the amide oxygen is thermodynamically favorable. The coordination of SOA ion group to the amide site is easily formed. There are three steps to be accomplished during the complexation process. The coordination compound is formed due to the electrostatic interaction, and the charge redistribution makes the energy reduce. Finally, the rotation of a branch is necessary to minimize the repulsion between the carbon-nitrogen chain and SC or SOA ion group for the final product structures.

V. ACKNOWLEDGMENTS

This work was supported by the Shandong Province Higher School Science and Technology Fund grant (No.J11LD11). Computation was supported in part by the Institute of Chemical Technology, Shandong University. The authors also thank Professor Yu-xiang Bu at Shandong University for valuable discussions.

[1] D. A. Tomalia, H. Baker, J. Dewald, and M. Hall, J. Polym. (Tokyo) **11**, 117 (1985).
[2] M. Zhao and R. M. Crooks, Adv. Mater. **11**, 217 (1999).
[3] M. Zhao and R. M. Crooks, Angew. Chem. Int. Ed. **38**, 364 (1999).
[4] K. Esumi, R. Isono, and T. Yoshimura, Langmuir **20**, 237 (2004).
[5] T. Jin, Appl. Mech. Mater. **217**, 252 (2012).
[6] L. Balogh and D. Tomalia, J. Am. Chem. Soc. **120**, 7355 (1998).
[7] L. Balogh, R. Valluzzi, K. S. Laverdure, S. P. Gido, G. L. Hagnauer, and D. A. Tomalia, J. Nanopart. Res. **1**, 353 (1999).
[8] S. Rajesh, A. M. Funston, P. Mulvaney, and R. W. Murray, Langmuir **25**, 13840 (2009).
[9] T. Jesionowski and A. Krysztafkiewicz, Colloids Surf. A **207**, 49 (2002).
[10] A. Manuel, M. Ricardo, and Z. Francisco, Appl. Catal. A **391**, 386 (2011).
[11] N. Tsubokawa, H. Ichioka, T. Satoh, S. Hayashi, and K. Fujiki, React. Funct. Polym. **37**, 75 (1998).
[12] S. Yoshikawa, T. Satoh, and N. Tsubokawa, Colloids Surf. A **153**, 395 (1999).
[13] H. Frank, M. Güngerich, P. J. Klar, and M. Fröba, J. Phys. Chem. C **111**, 5648 (2007).
[14] A. M. Kartal and C. Erkey, J. Supercrit. Fluids. **53**, 115 (2010).
[15] M. L. Saladino, A. Zanotto, D. C. Martino, A. Spinella, and G. Nasillo, Langmuir **26**, 13442 (2010).
[16] L. J. Wang, A. H. Lu, Z. Y. Xiao, and J. H. Ma, Appl. Surf. Sci. **255**, 7542 (2009).
[17] J. T. Park, J. A. Seo, S. H. Ahn, J. H. Kim, and S. W. Kang, J. Ind. Eng. Chem. **16**, 517 (2010).
[18] T. Jin, X. Li, and H. Sun, Int. J. Quantum Chem. **113**, 1213 (2013).
[19] B. Fubini, *In The Surface Properties of Silicas*, A. P. Legrand Ed., New York: Wiley, (1998).
[20] F. Hagelberg, J. Leszczynski, V. Murashov, and Z. Anorg, Allg. Chem. **454**, 209 (1998).
[21] G. Hochstrasser and J. F. Antoni, Surf. Sci. **32**, 644 (1972).
[22] V. Murashov, J. Mol. Struct. **650**, 141 (2003).
[23] C. C. Trout and J. D. Kubicki, J. Phys. Chem. A **108**, 1089 (2004).
[24] G. D. Zhou and L. Y. Duan, *Structural Chemistry*, Beijing: Peking University Press, (2007).
[25] D. Cakara, J. Kleimann, and M. Borkovec, Macromolecules **36**, 4201 (2003).
[26] T. V. Francisco and P. B. Balbuena, J. Phys. Chem. A **111**, 932 (2007).
[27] T. Jin and X. Li, Chin. J. Chem. Phys. **25**, 592 (2012).
[28] T. V. Francisco and P. B. Balbuena, J. Phys. Chem. A **112**, 4172 (2008).
[29] D. Astruc, E. Boisselier, and C. Ornelas, Chem. Rev. **110**, 1857 (2010).
[30] T. Jin and F. Zhang, Prog. Org. Coat. **72**, 447 (2013).
[31] I. Persson, P. Persson, M. Sandstrom, and A. S. Ullstrom, J. Chem. Soc. Dalton Trans. 1256 (2002).

DOI:10.1063/1674-0068/26/03/277-286